



Lead acid battery performance and cycle life increased through addition of discrete carbon nanotubes to both electrodes



Nanjan Sugumaran^a, Paul Everill^{a,*}, Steven W. Swogger^a, D.P. Dubey^b

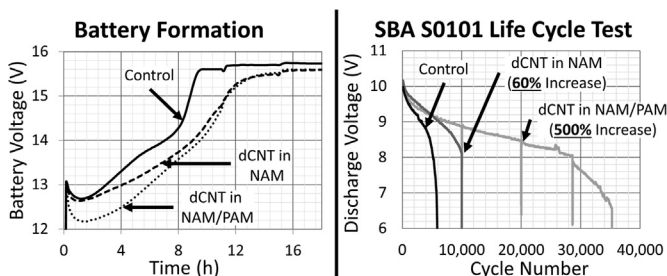
^a Molecular Rebar Design LLC, 13477 Fitzhugh Road, Austin, TX 78736, USA

^b Pacific Batteries Ltd., Lot 20/21, Wailda Industrial Estate, Lami, Fiji

HIGHLIGHTS

- Molecular Rebar[®] (discrete carbon nanotubes, dCNT) are formulated NAM/PAM additives.
- dCNT have no effect on paste density, rheology, or manufacturing processes.
- dCNT improve battery formation, maintain Reserve Capacity, and boost Cold-Crank.
- dCNT increase HRPSoc cycle life >60% and decrease water loss per cycle >19%.
- dCNT increase SBA S0101 cycle life >300% and decrease water loss per cycle >20–50%.

GRAPHICAL ABSTRACT



ARTICLE INFO

Article history:

Received 14 October 2014

Received in revised form

2 December 2014

Accepted 23 December 2014

Available online 24 December 2014

Keywords:

Carbon nanotube

Lead acid battery

Additive

Molecular Rebar[®]

SBA S0101

Hydrogen adsorption

ABSTRACT

Contemporary applications are changing the failure mechanisms of lead acid batteries. Sulfation at the negative electrode, acid stratification, and dendrite formation now precede positive electrode failures such as grid corrosion and active material shedding. To attenuate these failures, carbon has been explored as a negative electrode additive to increase charge acceptance, eliminate sulfation, and extend cycle life. Frequently, however, carbon incorporation decreases paste density and hinders manufacturability.

Discrete carbon nanotubes (dCNT), also known as Molecular Rebar[®], are lead acid battery additives which can be stably incorporated into either electrode to increase charge acceptance and cycle life with no change to paste density and without impeding the manufacturing process.

Here, full-scale automotive batteries containing dCNT in the negative electrode or both negative and positive electrodes are compared to control batteries. dCNT batteries show little change to Reserve Capacity, improved Cold Cranking, increased charge acceptance, and enhanced overall system efficiency. Life cycle tests show >60% increases when dCNT are incorporated into the negative electrode (HRPSoc/SBA) and up to 500% when incorporated into both electrodes (SBA), with water loss per cycle reduced >20%. Failure modes of cycled batteries are discussed and a hypothesis of dCNT action is introduced: the dCNT/H_{ad} Overcharge Reaction Mechanism.

© 2014 The Authors. Published by Elsevier B.V. This is an open access article under the CC BY license (<http://creativecommons.org/licenses/by/4.0/>).

* Corresponding author.

E-mail addresses: nanjans@hotmail.com (N. Sugumaran), peverill@molecularrebar.com (P. Everill), swwogger@molecularrebar.com (S.W. Swogger), dubey@pacificbatteries.com.fj (D.P. Dubey).

1. Introduction

In order to meet the demands of modern lead acid battery applications, the technology must provide higher levels of charge acceptance to boost system efficiency and delay common failure mechanisms such as sulfation or dendritic growth [1,2]. For example, in the modern automobile, advanced systems such as navigation, heating, and air conditioning can increase electrical energy consumption beyond that which the alternator can replenish during normal vehicle operation. The battery system therefore operates at a detrimental energy deficit. In order to maintain batteries at higher states of charge and avoid irreversible sulfation, modern applications demand increased charge acceptance. As a second example, batteries operating in hybrid-electric automobiles as well as some grid storage applications must be able to effectively accept charge in quick, high-current bursts or risk negative electrode passivation. If these challenges can be surmounted, lead acid batteries will remain competitive with other chemistries in the automobile, storage, and telecom markets, amongst others.

Carbon has been added to the Negative Active Material (NAM) during paste preparation in a variety of forms including carbon black, activated carbon, and more recently developed varieties including graphite and carbon nanotubes [6–8]. When incorporated at 0.1–6% w.r.t. lead oxide, carbon increases the charge acceptance of a battery by more than 200% but at the cost of paste rheology and paste density [3–5]. Reductions in paste density directly lead to decreased active material adhesion to the grids, decreased battery capacity which requires higher active material masses to reach specification, and insufficient cold-cranking performance [4]. New paste processing machinery is often required to overcome some of the issues brought on by high carbon loading. A further drawback to the use of carbon as a NAM additive is the potential to introduce gas-evolving impurities into the electrode. If the carbon additive is particularly high in iron residuals remaining from its production, for example, gas evolution and water loss will increase, leading to premature battery failure [9]. An abundance of literature studies discuss carbon allotropes, or mixtures thereof, in relation to the formation improvements [10] and charge acceptance boosts [6] they produce, but the detrimental effects of these carbon additives, namely paste property changes and gas evolution increases, remain consistent.

Our previous report introduced discrete carbon nanotubes (dCNT) as novel additives for the negative electrode [11]. The dCNT, also known as Molecular Rebar[®], are cleaned, functionalized, individualized, multi-walled, carbon nanotubes which are easily incorporated into battery pastes as a concentrated, pourable fluid [12]. The fluid replaces a portion of the water used during the paste mixing process, requiring no alteration to existing industrial production lines. When combined with traditional paste ingredients (lead oxide, expander, fiber, water, and acid) at 0.16% w.r.t. lead, dCNT offer prolonged increases in charge acceptance and more efficient battery usage with no detrimental effect to paste rheology or Reserve Capacity (RC), and an augmented Cold-Cranking Ability (CCA).

In this work, lead acid batteries incorporating dCNT into the negative electrode or both the negative and positive electrodes are compared to dCNT-free control batteries across various performance metrics. Addition of carbon additives to the positive electrode is typically avoided, with few exceptions [13], because of fears that the highly oxidizing environment of the positive electrode

would result in degradation of the carbon to carbon dioxide. Here, the stability of dCNT in such an environment is tested (See [supp. info.](#)) and the benefits of their inclusion in the Positive Active Material (PAM) is revealed. Full-scale, control batteries are compared to full-scale, experimental batteries containing 0.16% dCNT in the NAM or 0.16% dCNT in both the NAM and PAM. Pasting properties, basic performance (formation, reserve capacity, and cold temperature performance), advanced performance (polarization and triple electrode studies), gassing, cycle life (HRPSoC and SBA models), and battery failure mechanisms are presented.

dCNT provide additional benefits if added to both electrodes instead of the negative electrode alone. Batteries containing dCNT benefit from improved formation profiles, charge acceptance boosts of >200%, and elongated cycle life. Theories regarding the hydrogen adsorptive functionality of dCNT are introduced as a potential mechanism of action and grounds for future experimentation.

2. Experimental

2.1. Materials

Discrete carbon nanotubes (dCNT), also known as Molecular Rebar[®], are manufactured in Austin, Texas, by Molecular Rebar Design, LLC through a proprietary process that disentangles and functionalizes commonly available stock carbon nanotubes. Functionalization includes addition of carboxylic acid groups to the surface of the tubes and an increase in the number of open ends. The process also cleans the carbon nanotubes such that their residual catalyst content (Iron, Aluminum, etc.) drops ~80% from >5% by weight carbon to less than 1%, resulting in near pristine dCNT. A comparison of stock, non-processed carbon nanotubes and the dCNT can be found in our previous work [11].

The process by which the dCNT are prepared for use in lead acid batteries involves a surfactant coating step employing a high-intensity mixer. This produces a final, fluid dispersion of dCNT, surfactant, and water at a final concentration of 3% w/v dCNT at pH 7. This fluid is named Molecular Rebar[®] Lead Negative (MRLead⁻) or Molecular Rebar[®] Lead Positive (MRLead⁺) depending on its intended electrode, differentiated by processing methods and formulation.

Lead oxide (70% PbO/30% Pb) is manufactured onsite at Pacific Batteries, Ltd from 99.97% pure lead.

Hammond Expander is purchased directly from Hammond and used as per the manufacturer's instruction. Here, expander appropriate for SLI battery formulations is used (HEM-4640). The product includes proprietary amounts of barium sulfate (40–60%), sodium lignosulfate (25–40%), and carbon black (10–20%) [14].

All water used in the battery making process adheres to BS 4974:1975 standards.

Battery grade sulfuric acid (1.40 sp gr.) is used during paste mixing.

2.2. Scanning electron microscopy

High resolution scanning electron microscopy is accomplished with a Jeol JSM-6010LV instrument.

Battery plates are prepared for SEM analysis by removing them from their battery casings, washing them with distilled water until the runoff is pH neutral, and then drying them under vacuum at 30–40 °C. Samples are obtained by carefully pushing the dried

plate material out of the grid by finger, preventing damage to the outward-facing surface as much as possible. Finished samples resemble small 3–4 × 8–10 mm rectangles, about 2 mm thick. A small piece of double-sided carbon tape is used to secure a portion of the material to a sample platform such that the sample reveals one of the outward-facing surfaces, not the surfaces previously in contact with the grid.

dCNT or Carbon Black SEM samples are mixed using 3–5 mg of either compound combined with 5–10 mL of water or methanol in a small, glass vial. The sample is exposed to 2–3 min of bath sonication to aid in mixing. After this period, the sample forms a uniform gray–black fluid which is substantially free from particulates. A single drop of the sample is placed on a silicon wafer and air dried, removing all liquid. The wafer is fixed to a sample platform with colloidal graphite.

Images are typically resolved at 5–20,000× magnification with a spot size of 20–30 and a beam strength of 10–15 kV.

2.3. Negative and Positive Active Material paste mixing and analysis

dCNT are provided as aqueous dispersions, MRLead– or MRLead+, allowing them to be uniformly distributed in NAM or PAM paste mixes. During regular pasting procedures, a specific volume of water, X, is added to dry ingredients such that appropriate paste density specifications are met. In order to conserve paste consistency, the volume of MRLead– or MRLead+, Y, added to the paste is displaced from volume X to result in the remaining water allowance volume, Z, such that $X = Y + Z$. The MRLead– or MRLead+ volume, Y, is added to the dry mixture first, followed by the remaining water allowance, Z, in order to maintain the liquid portion of the paste at volume X.

Large-scale NAM paste mixes comprising 230 kg lead oxide, 0.15 kg Dynel fiber, and 1.4 kg Expander are combined mechanically as 27.0 L water (Control) or 14.5 L water and 12.5 L MRLead– (Experimental) are added. When a paste forms, 23.1 kg sulfuric acid (1.4 sp gr.) is added to form the completed, pasteable dough.

Large-scale PAM paste mixes comprising 230 kg lead oxide and 0.15 kg Dynel fiber are combined mechanically as 30.0 L of water (Control) or 17.5 L water and 12.5 L MRLead+ (Experimental) are added. When a paste forms, 25.9 kg sulfuric acid (1.4 sp gr.) is added to form the completed, pasetable dough.

Paste density is measured by density measuring cup.

Penetration is measured by Humboldt penetrometer.

2.4. Plate curing, battery manufacture, and formation

After paste mixing, the material is pasted onto lead grids containing 1.7% Antimony and subsequently exposed to a standard curing/drying procedure resulting in finished plates with <1% free lead and <1% moisture.

After drying, experimental NAM plates contain a final dCNT concentration of 0.16%, a final barium sulfate concentration of 0.24–0.37%, a final sodium lignosulfonate concentration of 0.15–0.24%, and a final carbon black concentration of 0.06–0.12%, all w.r.t. the weight of lead oxide. Experimental PAM plates contain 0.16% dCNT w.r.t. lead, but lack expander components. Control plates are prepared identically, with the omission of dCNT.

Control NS40 batteries (4 positive and 5 negative plates) batteries, NS40 batteries with dCNT in negative plates, and NS40 batteries with dCNT in positive and negative plates are produced at Pacific Batteries Ltd. (Lami, Fiji) and shipped to an independent battery research laboratory, JBI Corporation (Ohio, USA), for formation and testing. NS40 are classified as 12 V automotive batteries rated with 50 min Reserve Capacity, 35 A h C_{20} rate, and 270 s cold-

crank performance. Dimensions are: length, 197 mm; width, 129 mm; and height, 230 mm.

Batteries are flooded and formed at the JBI Corporation using 7 A constant current over 18 h. Voltage evolution is monitored every 10 min. Formation data is the average of 5 concurrently tested batteries.

2.5. Basic battery performance testing

All battery data is an average of 5–15 concurrently tested batteries. Prior to testing, all batteries are fully charged using a constant voltage of 14.8 V and a limiting current of 8 A for 20 h. Batteries are allowed to cool for 4 h prior to use.

Freshly formed batteries are subjected to alternating cycles of reserve capacity and cold-cranking measurement. A total of three cycles (3 RC and 3 CCA) are presented.

2.5.1. Reserve Capacity test

Batteries are discharged at 25 A constant current until voltage decreases to 10.5 V. Time is measured. Prior to cold-cranking tests, batteries are recharged using 14.8 V constant voltage with a limiting current of 8 A for 20 h followed by a 4 h cooling period.

2.5.2. Cold-Cranking Ability tests

Batteries are discharged at -18°C with a 270 A constant current. The voltage after 30 s is measured. Additionally, the length of time required to discharge the battery to 6.0 V is also measured. After this test, batteries are recharged using 14.8 V constant voltage with a limiting current of 8 A for 12 h.

2.5.3. Cold charge acceptance

Fully charged batteries are discharged at a constant current of 3.5 A for 5 h, until they reach 50% State of Charge (SoC). Batteries are then cooled to 0°C over 18 h. Charging proceeds at a constant voltage of 14.4 V with current input being measured for 10 min. Curve shape, current end point, and A/h forced into the battery are examined.

2.6. Advanced battery performance testing

Polarization tests at 100% state of charge are conducted after the Battery Testing Regimen described in Section 2.5. Prior to tests, all batteries are fully charged using a constant voltage of 14.8 V and a limiting current of 8 A for 20 h. Batteries are cooled for 4 h prior to use. All data represents an average of five concurrently tested batteries.

2.6.1. Constant current polarization tests

In constant current studies, a set current is passed through fully charged batteries for 5 min during which time the voltage is measured. After the first 5 min, the current is raised, and voltage is measured again for an additional second 5 min period. This protocol repeats for a total of 10 measurements. Here, the current profile begins at 0.2 A and rises in 0.2 A increments until a final current of 2.0 A is reached.

A Tafel Plot is extrapolated from the above data set using the calculated overvoltage at each 5 min period versus the logarithm of the current over that particular period. Although steady-state conditions are best measured after a period of many hours, or perhaps days, here, a shorter 5 min period was used. The interval was sufficient to lower the change in voltage per unit time to less than a twentieth of its initial value and provide a reasonable approximation of the steady-state condition. Lines of best fit are calculated for $x > -0.4$ and slopes are reported.

2.6.2. Constant voltage polarization tests

In constant voltage studies, a set voltage of 13.0 V is placed over fully charged batteries with a limiting current of 7 A applied. Current is monitored for 5 min and then the voltage is increased by 0.3 V. Current is monitored again for 5 min, and successive 0.3 V boosts are repeated until a final voltage of 15.4 V is reached.

Steady-state constant voltage tests, are extrapolated from the above data set using the final current measurement of each 5 min period versus the voltage of that particular period.

2.7. Gassing tests

After basic battery tests are complete (Section 2.5), water is topped off as required and batteries are placed in a 51.7 °C water bath according to SAE J 537 protocols. Batteries are charged for 16 h at 14.1 V constant voltage. Batteries are charged for an additional 4 h at 14.1 V and the volume of gas produced over the last 30 min is measured via a burette hermetically attached to the battery vent. The current and total A·h across the battery is also monitored.

For comparison, this test is also run at a constant voltage charge of 13.6 V.

2.8. Cycle life testing

2.8.1. High-Rate Partial-State-of-Charge (HRPSoC) life cycle model (microhybrid)

Fully charged batteries (described in Section 2.4) with and without dCNT incorporated into their negative or negative and positive electrodes are discharged for 3 h at 3.5 A. Batteries are then charged at 42 A for 60 s, rested for 10 s, discharged at 42 A for 60 s, and rested for an additional 10 s. This charge–rest–discharge–rest cycle is completed an additional 3999 times, or until the charging voltage is >16.98 V or the discharging voltage is <10.38 V. If the battery reaches 4000 repeats, the battery is recharged for 20 h at a constant voltage of 14.8 V with a limiting current of 8 A so Reserve Capacity (described in Section 2.5.1) can be measured to ensure battery health. The battery is then recharged again (14.8 V, 8 A limit, 20 h) and the complete protocol is repeated an additional three times for a possible cumulative total of 16,000 cycles, if the batteries successfully endure.

2.8.2. SBA S0101 model (idling start–stop)

Fully charged batteries (described in Section 2.4) are discharged for 59 s at 35 A and then for 1 s at 235 A. The battery is then charged at 14 V constant voltage with a limiting current of 78 A. This discharge–discharge–charge cycle is repeated until the end of discharge voltage is <6.0 V. Typically, this test runs for tens of thousands of cycles but, importantly, was developed for the testing of cutting-edge lead acid batteries.

2.8.3. Cadmium electrode studies

A cadmium rod reference electrode is introduced to a control or experimental battery during HRPSoC duty cycle after the 10th cycle post-full recharge. Voltage is measured against the negative or positive electrode between the 55th and 60th second of the charging step. This measurement is repeated 5–6 times for consistency.

2.8.4. Failure analysis

Modes of failure are assessed after cycling tests by JBI Corporation (Ohio, USA) according to BCI standards.

Water loss per cycle measurements are extrapolated from decreases in battery weight and the total number of cycles achieved by the battery under each test.

SEM images of failed battery plate materials are collected as in

Section 2.2.

3. Results

3.1. Effect of dCNT on paste rheology and consistency

Addition of excess carbon to paste mixtures typically requires the addition of excess water to complete paste formation [6]. Negative effects of this addition include decreased paste density, decreased paste-grid adhesion, and alterations to the manufacturing process to accommodate these changes. NAM and PAM paste mixtures including dCNT at a final concentration of 0.16% w.r.t. the weight of dry lead oxide were produced and compared with dCNT-free control paste mixtures to screen for these effects. No paste mixture containing dCNT required the addition of excess water over that required by the paste formulations described here.

Paste parameters include density and penetration. Control NAM paste show densities of $4.26 \pm 0.02 \text{ g mL}^{-1}$ which is statistically indistinguishable from the density of experimental NAM paste mixtures comprising 0.16% dCNT, w.r.t lead oxide, measuring $4.25 \pm 0.02 \text{ g mL}^{-1}$. Paste penetration is identical between control and experimental NAM paste batches, measured at 19 units. In regard to the PAM paste mixture, control batches produce densities of $4.07 \pm 0.02 \text{ g mL}^{-1}$ while experimental batches measure $4.10 \pm 0.02 \text{ g mL}^{-1}$. Paste penetration is, again, identical between controls and experimental batches, measured at 18 units.

Reiterating our previous findings [11], dCNT produce no significant changes to negative, and now positive, paste rheology, density, or penetration parameters. dCNT, therefore, can be incorporated into existing paste manufacturing processes with no significant alteration, mechanical or procedural.

3.2. Effect of dCNT on negative and positive electrode formation

Shown in Fig. 1A are the constant-current formation profiles of control batteries and batteries containing dCNT in the negative, or negative and positive, electrodes. Over the course of an 18 h, 7 A constant-current formation a significant drop in charging voltage is observed across all batteries containing dCNT.

By virtue of the decreased voltages and subsequent shifting of the formation curve, the time taken to reach gassing voltages is delayed. The oxygen gassing potential (14.4 V) is delayed ~2 h when dCNT are added to the negative electrode alone, and 2.5 h when dCNT are present in both electrodes. Similarly, the hydrogen gassing potential (>15.6 V) is delayed 5.6 h when dCNT is incorporated into the negative electrode. These delays are reiterated in the derivative plot ($\partial V/\partial t$) shown in Fig. 1B. Given the lower voltage formation of batteries containing dCNT, it could be possible to increase the formation current while maintaining voltages similar to, or lower than, control batteries. A formation profile testing this hypothesis would achieve the same total A·h-in over a shorter time and could, perhaps, be used to increase manufacturing output.

dCNT incorporated into the positive electrode produce distinct changes in the first 6 h of formation, indicating efficient conversion of the positive electrode. dCNT incorporated into the negative electrode produce changes in voltage–time profiles towards the end of charging that allude to changes in hydrogen evolution mechanisms potentially responsible for the high cycle life of dCNT containing batteries, to be discussed later.

3.3. Effect of dCNT on basic battery performance parameters

Reserve Capacity measures the length of time a battery can produce a “meaningful” current until its voltage drops below a certain threshold value, in this case 10.5 V. Frequently, carbon

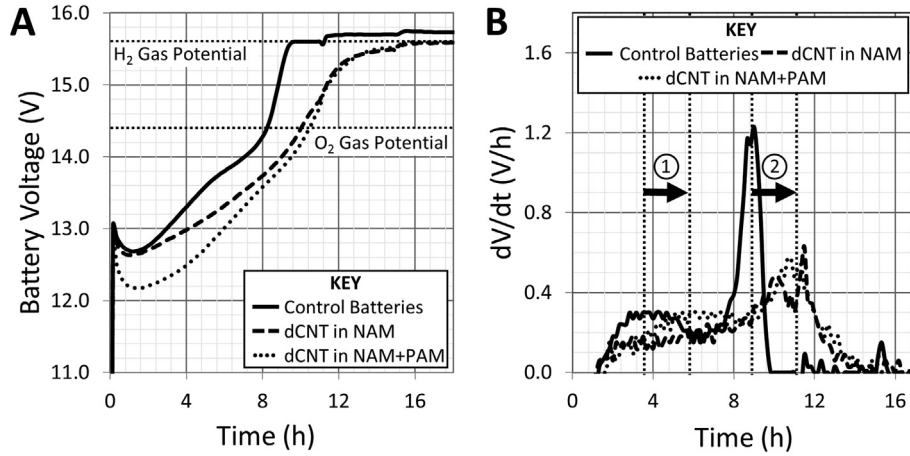


Fig. 1. Effect of dCNT on formation profiles. A) Voltage vs. time profiles over the course of an 18 h, 7 A constant-current formation show decreased voltages in batteries containing dCNT. B) A derivative plot ($\delta V/\delta t$) highlights two shifts in activities occurring during formation. Shift 1 occurs when dCNT are present in the positive electrode, indicating ease of positive electrode conversion, while Shift 2 occurs when dCNT are present in the negative electrode, indicating altered overcharge reactions.

additives detrimentally effect this parameter and fail to meet manufacturer's specifications. Fig. 2A shows that, over the course of three cycles, the presence of dCNT in the negative, or negative and

positive, electrode do not hinder this parameter. Although differences between batteries are negligible, dCNT in the NAM, alone, appear to have the best effect.

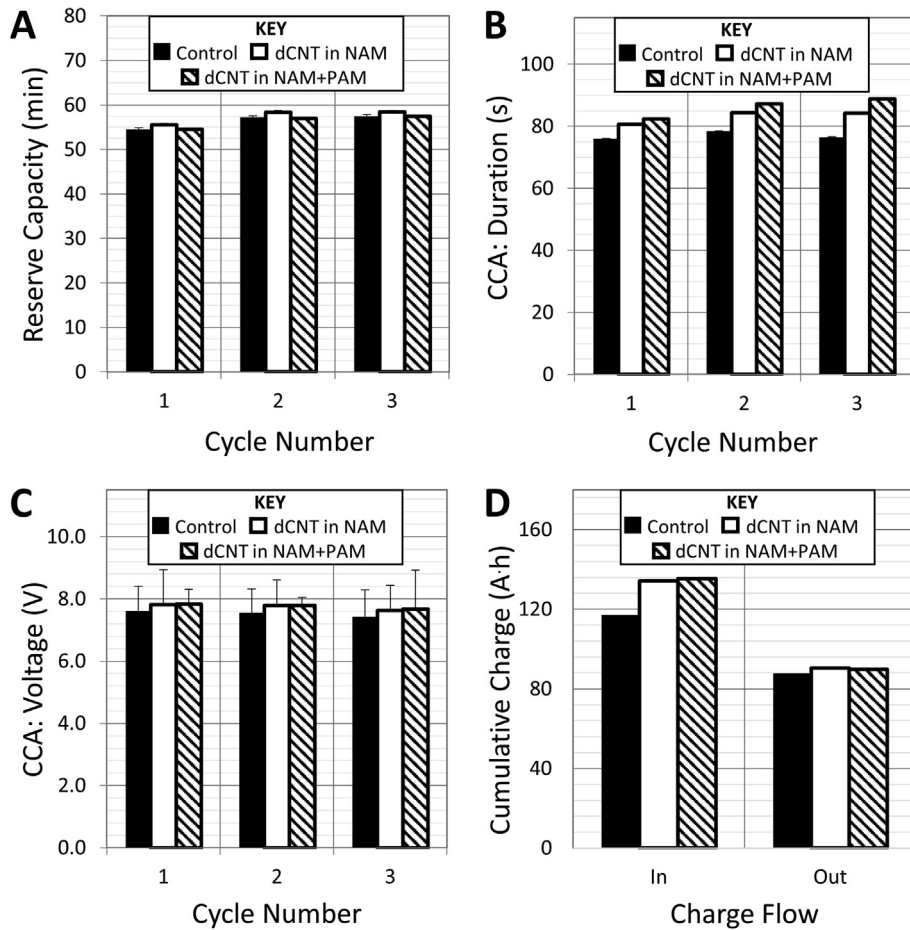


Fig. 2. Effect of dCNT on Basic Battery Performance Parameters. A, Reserve capacity tests (25 A discharge until voltage <10.5 V) show batteries containing dCNT perform similarly to Control batteries. B, Cold-cranking, durational tests (270 A discharge until voltage <6 V at $-18\text{ }^{\circ}\text{C}$) show improvement when dCNT is incorporated at the negative electrode and a greater improvement when incorporated in both electrodes. C, Cold-cranking, voltage tests (270 A discharge at $-18\text{ }^{\circ}\text{C}$, voltage read at 30 s) show little change between batteries containing dCNT and controls. D, The cumulative charge factor shows batteries containing dCNT in the negative electrode or the negative and positive electrode absorb >15% more energy and pass >4% more charge than dCNT-free controls.

Cold-cranking measurements differentiate dCNT from other advanced carbons by increasing the duration which a battery can hold a high current discharge at -18°C . Fig. 2B indicates that dCNT added to the negative electrode increase the duration of current flow by $>6\%$ but, if added to both electrodes, a synergistic effect is observed producing a $>13\%$ increase. Comparison of the voltage produced at the 30 s point of a high, 270 A current discharge shows no detrimental effect of dCNT as negative, or negative and positive, electrode additives (Fig. 2C).

Total charge, measured in A·h, is quantified for all batteries during the three RC-CCA cycles, summed, and presented in Fig. 2D. dCNT increase the amount of charge flowing into the battery by $>15\%$ when incorporated into the negative, or negative and positive, electrode over identical charging and discharging protocols, described in the Section 2.5.

As the increase in cold-cranking duration with carbon additives is an unexpected result, we investigated whether dCNT increase current acceptance under cold conditions. For this test, batteries discharged to 50% SoC are cooled to a 0°C internal temperature prior to a 14.4 V constant voltage charge. Fig. 3 shows that dCNT increase current acceptance in cold temperature (0°C) environments when incorporated into the negative electrode, and increases acceptance further when incorporated into both electrodes. After 10 min (600 s) of charge, control batteries are passing 6.69 A while batteries containing dCNT in the negative electrode are passing 7.55 A (12.8% increase) and batteries containing dCNT in both electrodes are passing 7.96 A (19.0% increase). Area-under-the-curve calculations show that dCNT batteries accept 4–6% more charge than control batteries over the same period. Interestingly, when dCNT are incorporated in both electrodes, the cold charge acceptance appears to trend upwards as the test continues; an observation not apparent when dCNT are included in the negative electrode only. This trend is surprising and could be the result of unforeseen temperature increases during the course of the study, either environmental or internal. Increased current translates directly into increased A·h values indicating that dCNT batteries have better charge acceptance in cold conditions.

In contrast to other carbon additives, dCNT produce comparable or improved results in Reserve Capacity and Cold-Cranking tests. Furthermore, batteries incorporating dCNT have augmented low-temperature performance that can lead to faster charging and

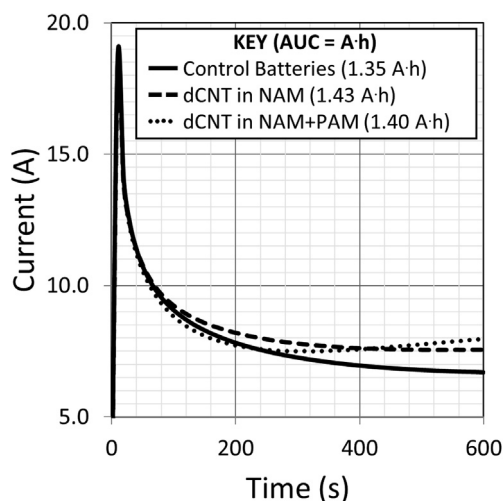


Fig. 3. Effect of dCNT on cold charge acceptance. Batteries containing dCNT in the negative electrode or in both electrodes absorb more current than CNT-free control batteries when charged from 50% SoC at a constant voltage of 14.4 V in 0°C temperatures.

longer periods of utilization in such environments.

3.4. Effect of dCNT on advanced battery performance parameters

In an effort to understand the effect of dCNT on battery performance, constant-current and constant voltage experiments are presented.

Fig. 4A shows the voltage performance of various batteries held under various constant current steps leading from 0.2 to 2 A in 0.2 A, 5 min steps. Batteries incorporating dCNT in the negative electrode are capable of handling the same current as controls, but at lower voltages. This concept is reiterated in the Tafel Plot in Fig. 4B where changes in line shape and slope indicate changes in the chemistry occurring on the electrode surface during over-voltage charging. The drops in voltage seen at each current step highlight the decreased charge transfer resistance and increased current flow of systems containing dCNT over controls. The slope of the best fit lines through data points where $x > -0.4$ are calculated: control = 3.46 (576 mV/cell), dCNT in the negative electrode = 2.49 (415 mV/cell), and dCNT in the negative and positive electrodes = 2.24 (373 mV/cell). dCNT are found to decrease the Tafel Slope. The shape of each voltage step in Fig. 4A indicates the Tafel slope could be related, in part, to a change in the mechanism of hydrogen evolution on the dCNT. It is possible this change could involve dCNT adsorption of hydrogen, to be discussed later.

In the constant-voltage polarization test of Fig. 4C, batteries containing dCNT in the negative electrode are shown to pass higher current for a given voltage than controls. A further increase is seen when dCNT are included in both negative and positive pastes. As in our previous paper, the high-current influxes observable in the first few seconds of charging highlight the fast-acting pseudocapacitance of the dCNT in overcharge regimes. The effects of dCNT addition are reiterated in Fig. 4D which reinterprets the data in Fig. 4C at steady-state conditions. As opposed to other forms of carbon, the boost in current is maintained for the duration of each voltage step, instead of dropping off to control levels after a few seconds.

dCNT imbues lead acid batteries with the ability to produce less overvoltage for a given current and, conversely, produce higher current at a given overvoltage. As these results originate from fully-charged batteries, changes in performance reflect differences in side reaction kinetics and, importantly, inform us of ways to mediate them. Fig. 4C, for example, indicates that batteries containing dCNT in the positive and negative electrodes pass similar current at 13.9 V as control batteries at 14.5 V. Batteries containing dCNT, therefore, could be recharged at lower voltages than control batteries to reach identical A·h-in parameters more efficiently.

3.5. Effect of dCNT on gassing and water loss

Carbon additives typically increase outgassing and it is important to determine whether dCNT also suffers from this limitation.

Fig. 5A indicates that dCNT increase gas evolution under standard, 14.1 V gassing tests. However, this isolated observation results in an incomplete picture. Measurement of the current observed at the end of the 30 min gas-gathering experiment shown in Fig. 5B indicates that batteries containing dCNT in the negative or the negative and positive electrodes are channeling almost double the current of control batteries. These batteries therefore accept more A·h when compared to their control counterparts, all of which goes directly into gas-evolving side reactions. Control batteries receive 0.16 A·h over the 30 min gas-monitoring period while batteries with dCNT incorporated in the negative, or negative and positive, electrodes receive 0.32 A·h. If gas output per cell is normalized to the A·h received per cell, control batteries produce 316.9 mL gas/A·h

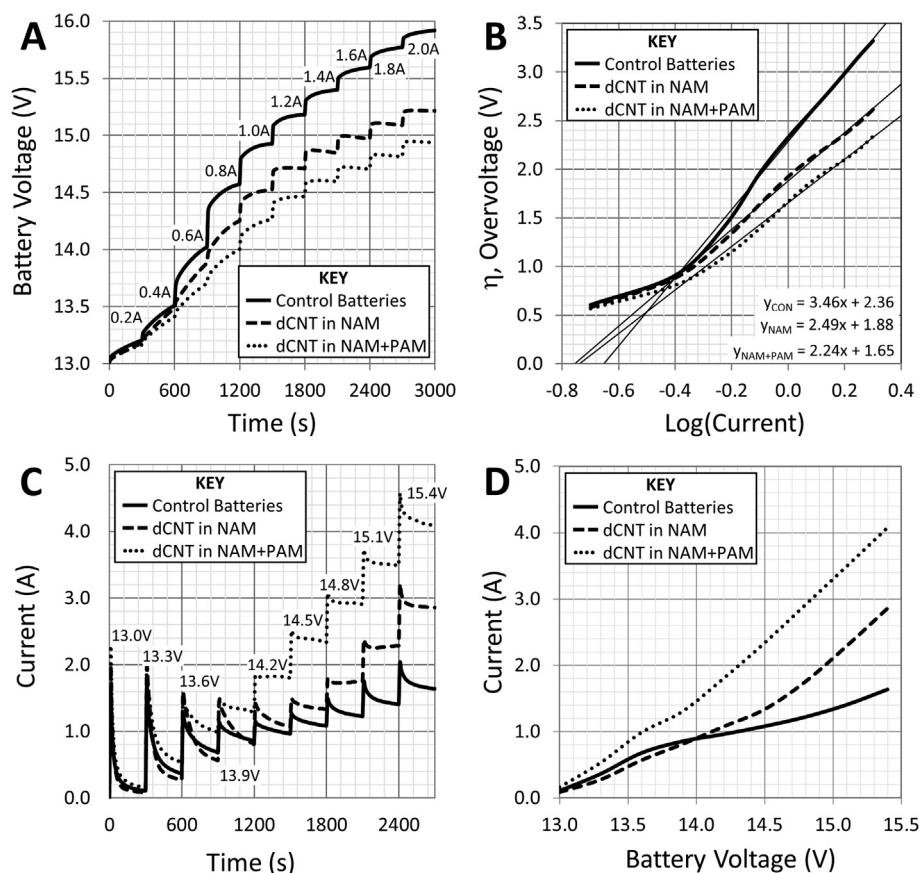


Fig. 4. Effect of dCNT on Advanced Battery Performance Parameters. A, Constant-current studies (voltage measured, current increased from 0.2 to 2 A in 0.2 A, 5 min increments) indicate that batteries containing dCNT exhibit less overvoltage when incorporated into the negative electrode than control batteries and even lesser overvoltage when incorporated into both electrodes. B, A Tafel Plot highlighting the difference in overvoltage processes between each battery variety. Lines of best fit are drawn through the linear portion of the data with equations shown. C, Constant-voltage studies (current measured, voltage increased from 13 to 15.4 V in 0.3 V, 5 min increments) indicate that batteries containing dCNT produce higher current when incorporated into the negative electrode than controls, and even higher current when incorporated into both electrodes. D, Steady-state, constant-voltage studies reiterate the current increases observed in C.

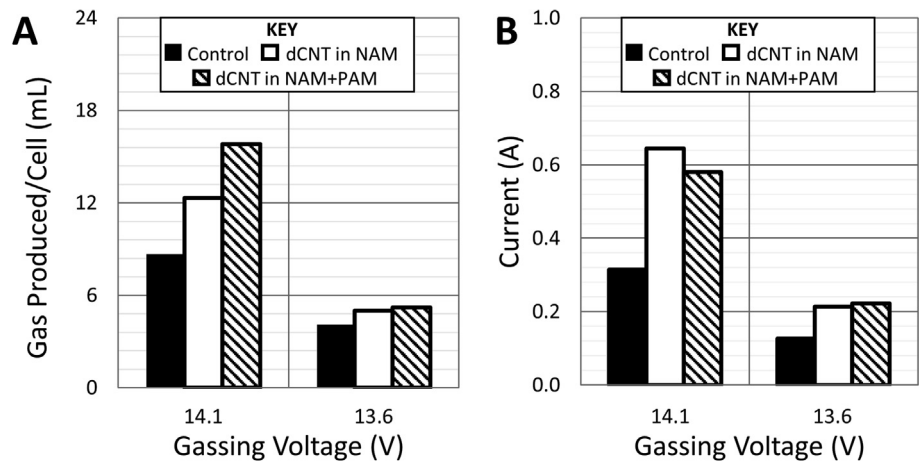


Fig. 5. Effect of dCNT on Gassing and Water Loss. A, Addition of dCNT to the negative or negative and positive electrodes produces ~40–80% increases in gas production per cell. B, Batteries containing dCNT pass more current than control batteries during this test.

while batteries containing dCNT in the negative electrode produce 231.2 mL Gas/A·h (27% decrease vs. control batteries) and batteries containing dCNT in both electrodes produce 296.8 mL Gas/A·h (6% decrease vs. control batteries). This suggests that batteries containing dCNT can produce less gas than control batteries when A·h-

is controlled, either through voltage decreases or tight A·h-in control. In ideal conditions, Faraday's Law predicts gas evolution should be 626 mL/A·h, but this number is unachievable here because a portion of gas remains trapped between the top of the battery case and the top of the acid. It is possible that a portion of

the gas deficit observed in batteries containing dCNT is due to hydrogen adsorption on the surface of the dCNT, a theory to be discussed later.

The standard gassing test was rerun at a lower 13.6 V to mimic more contemporary battery applications and test our theory concerning lower charging voltages as an option to manage gas production. At this lowered voltage, gas production from batteries containing dCNT was still higher than controls, but the current passing at the 30 min mark in batteries containing dCNT in the negative, or the negative and positive, electrode is similar to control batteries charging at the higher 14.1 V, corroborating our theory.

dCNT changes the nature of lead acid batteries. Increased charge acceptance and alteration of the electrode surface chemistry require additional attention to side-reaction management. A battery containing dCNT charges faster than a conventional battery, obviating the need for elongated recharge periods, especially on float. Similarly, a battery containing dCNT charges fully at lower voltage than a conventional battery making recharge protocols operating at >14.8 V at not required. New battery management systems or updated industry specifications may be required to take full advantage of batteries containing dCNT. There is precedence for altered battery charging protocols: the industry had to make significant updates during the switch from Antimony to Calcium grid alloys, for example.

3.6. Effect of dCNT on HRPSoC cycle life (micro-hybrid model)

An established model for microhybrid automotive battery usage

is the High-Rate Partial-State-of-Charge protocol, or HRPSoC [15]. Fig. 6A shows the performance enhancement dCNT bring to batteries containing the additive in their negative electrode when compared to controls. The somewhat simple NS40 batteries used here are not built to undergo these tests and they do not complete 4000 cycles before the End of Discharge (EOD) voltage limit (10.38 V) is reached. Batteries incorporating dCNT in the negative electrode reach 4000 cycle limit for the second round of cycles and the battery containing dCNT achieves a further 6648 cycles before the EOD limit is reached. At each segment, batteries containing dCNT in the negative electrode enjoy higher cycle numbers than controls before lower voltage limits are reached (Fig. 6C), ending with a combined 60% increased cycle life over control batteries (12,044 vs. 18,901 cycles).

Fig. 6B highlights a similar ~0.6 V drop in charging voltage over set currents identified in formation and polarization studies. At constant current, batteries with dCNT produce lower observed voltages underscoring their efficiency and facile charge acceptance.

The Reserve Capacity tests built into each of the four HRPSoC segments, shown in Fig. 6D, indicate that batteries containing dCNT remain in better health than control batteries throughout the test.

Fig. 7 shows the results of a cadmium reference electrode study conducted during a section of the HRPSoC duty cycle. In both the positive and negative electrode studies, a depolarizing behavior can be seen. The data suggest that effects of dCNT propagate to the counter electrode, possibly indicating an improved formation or a reduction in concentration polarization during charging and

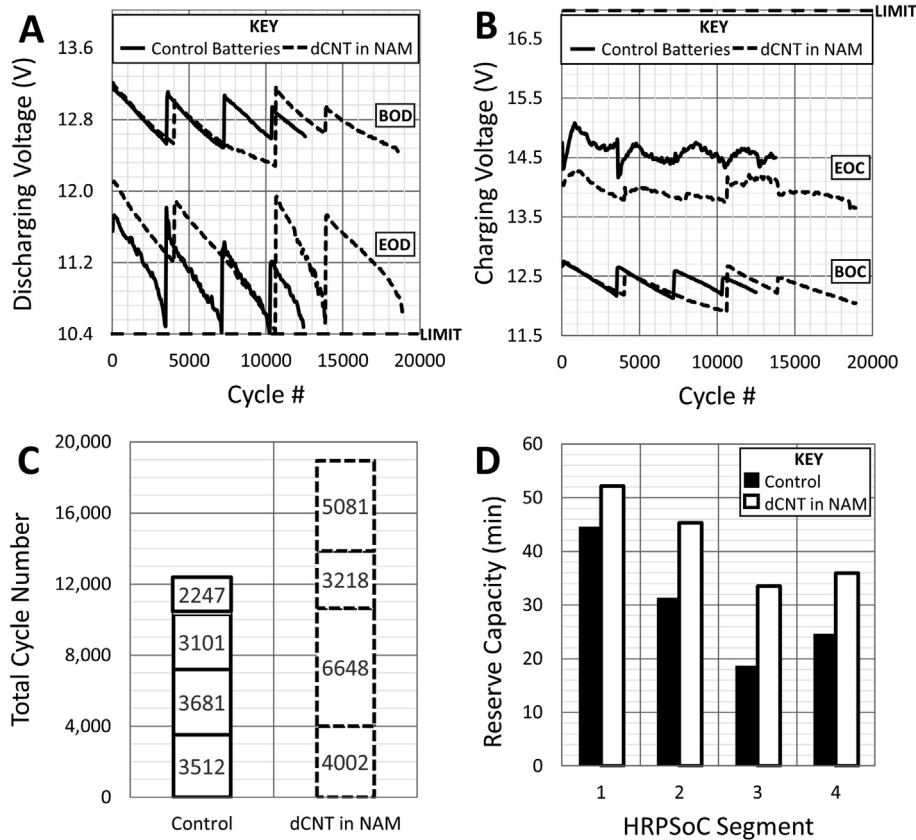


Fig. 6. Effect of dCNT on Cycle Life, High-Rate Partial-State-of-Charge (HRPSoC). A, Beginning and end of discharge voltages are shown with the 10.38 V limit indicated. B, Beginning and end of charge voltages with the 16.98 V limit indicated. A drop in EOC is observed in batteries containing dCNT, consistent with earlier results. C, Graphical representation of cycle numbers measured at each HRPSoC segment. D, Reserve Capacity measurements taken after each segment show dCNT containing batteries remain healthier than controls throughout the experiment.

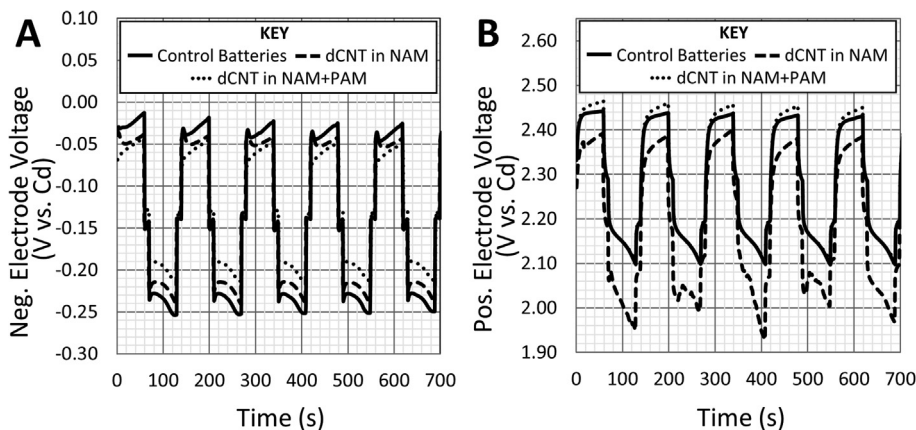


Fig. 7. Effect of dCNT on Each Electrode, Cadmium Reference Study. A depolarizing effect is seen in both electrodes with the addition of dCNT to the negative, or negative and positive electrodes. In Figure B, the lower NAM + PAM data points are hidden by the Control battery data.

discharging. In the negative electrode, the depolarizing behavior of dCNT could potentially be due to a change in the hydrogen evolution mechanisms while in the positive electrode, the dCNT may be acting to preserve surface area throughout cycling. Further study is required to confirm these hypotheses.

Teardown analysis indicated that sulfation of the negative electrode is the predominant failure mode for these batteries, as confirmed by SEM (Fig. 8). During sample preparation, all plates containing dCNT proved less crumbly and stronger to the touch than control plates which highlights the increased mechanical strength and grid adhesion properties of dCNT-laced active material. Sulfation is observed at the control negative electrode as long, >50 μm , acicular lead sulfate crystals (Fig. 8A). These needle-like crystals appear to be covering a layer of more regular, boulder-

like, lead crystals suggesting a passivating layer may have formed over the surface of the plate. The morphology of the negative electrode containing dCNT is different, containing shorter, <10 μm lead sulfate crystals which appear to be more ordered and uniform than crystals observed in the control electrode (Fig. 8B). This suggests, but does not prove, that dCNT could be affecting crystal nucleation. Similarly, when comparing the positive electrode surfaces (Fig. 8C and D), a fluffy, moss-like morphology is apparent in the control image which contrasts with the more ordered nature of the dCNT image. Again, a relationship appears to exist between dCNT incorporation and decreased crystal size. For further interpretation of the effect of dCNT on plate structure and morphology, surface area and porosity measurements will be included in future research.

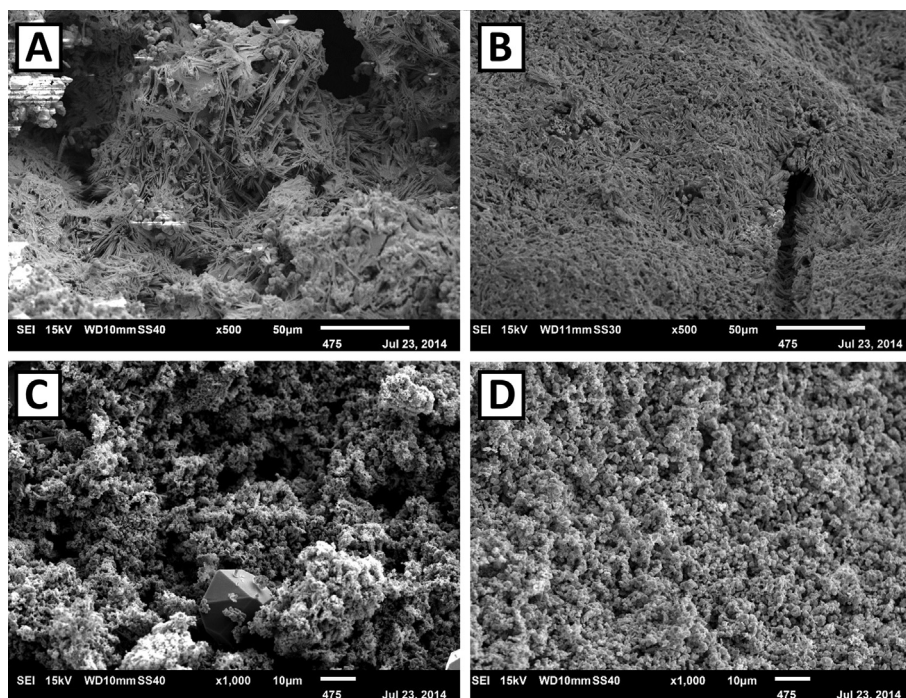


Fig. 8. SEM analysis of failed batteries from HRPSoc Duty Cycles. A, Control, negative electrode (~12 k cycles) showing heavy growth of acicular crystals. B, dCNT-containing, negative electrode (~19 k cycles) showing tight crystalline arrangement and a well-structured surface. C, Control, positive electrode (~12 k cycles) showing a large and non-uniform variety of crystals. D, Positive electrode from a battery containing dCNT in the negative electrode (~19 k cycles) showing small, well defined crystals retaining a uniform structure. A and B are 500 \times while C and D are 1000 \times magnification.

Total battery weight before and after cycling is compared in light of the number of cycles each battery attained. Control batteries lose 0.018 g/Cycle while batteries containing dCNT lose 0.015 g/Cycle; a 20% decrease in water loss. Improved water loss is likely an upshot of the decreased charging voltage that dCNT permits when included in the negative electrode or, perhaps, a degree of hydrogen adsorption on the surface of the dCNT.

By cycling more efficiently through increased charge acceptance and ease of discharge, cycle life and water retention of batteries containing dCNT are greatly enhanced over control batteries in HRPSoC duty modes.

3.7. Effect of dCNT on SBA modeled cycle life (idling start–stop model)

An established model for testing idling start–stop functionality is the Japanese SBA S0101 standard [16]. This test is more aggressive than the HRPSoC cycling model and designed largely for advanced batteries. Here, dCNT elevates the performance of simple, flooded automotive batteries to a tier usually only reached by those advanced batteries. Fig. 9A shows that incorporation of dCNT into the negative or positive electrodes allows a battery to reach 9999 or 35,300 cycles, respectively. When compared to the control battery reaching 5883 cycles, this represents a 60% or 500% increase in lifetime. The benefit of adding dCNT to both negative and positive electrodes is clear.

Fig. 9C presents data from 3 batteries as a horizontal average with vertical bars drawn to encompass all measured data points.

The variability of control batteries is small because they were limited by electrochemical failures. The variability of batteries containing dCNT in the NAM, or the NAM and the PAM, is larger because the failure mode was not electrochemically based, rather, the batteries with dCNT failed due to an eventual mechanical failure.

Teardown analysis of SBA-cycled batteries revealed an unexpected potential failure mode in batteries containing dCNT: separator failure. NS40 batteries are not built to sustain SBA cycling conditions and it is interesting to note that inclusion of dCNT in the electrodes prevented active material failure and switched the failure mode to more physical, manufacturing-based mechanisms. In batteries containing dCNT, the separators switched from their normal elastic nature to a harder, more brittle form that led to battery failure and positive material problems. Sulfation on the negative electrode was not observed in SEM micrographs (Fig. 10A and B) but a change in crystal structure reminiscent of differences observed in HRPSoC cycles plates was apparent. Crystals populating the control negative electrode surface appear to be of various sizes and shapes; non-uniform in morphology. Electrodes containing dCNT are easily contrasted to controls by virtue of their high degree of uniformity. Whereas crystals observed in control electrodes are between 1 and 20 μm , crystals in dCNT electrodes form within a tighter range, between 5 and 10 μm . In the positive electrode, control crystals appear to fall into two groups: small, <3 μm crystals and much larger >10 μm crystals (Fig. 10C and D). The crystals observed in the dCNT positive electrode appear “feathered”, having less defined edges, and are more homogenous, being of the same

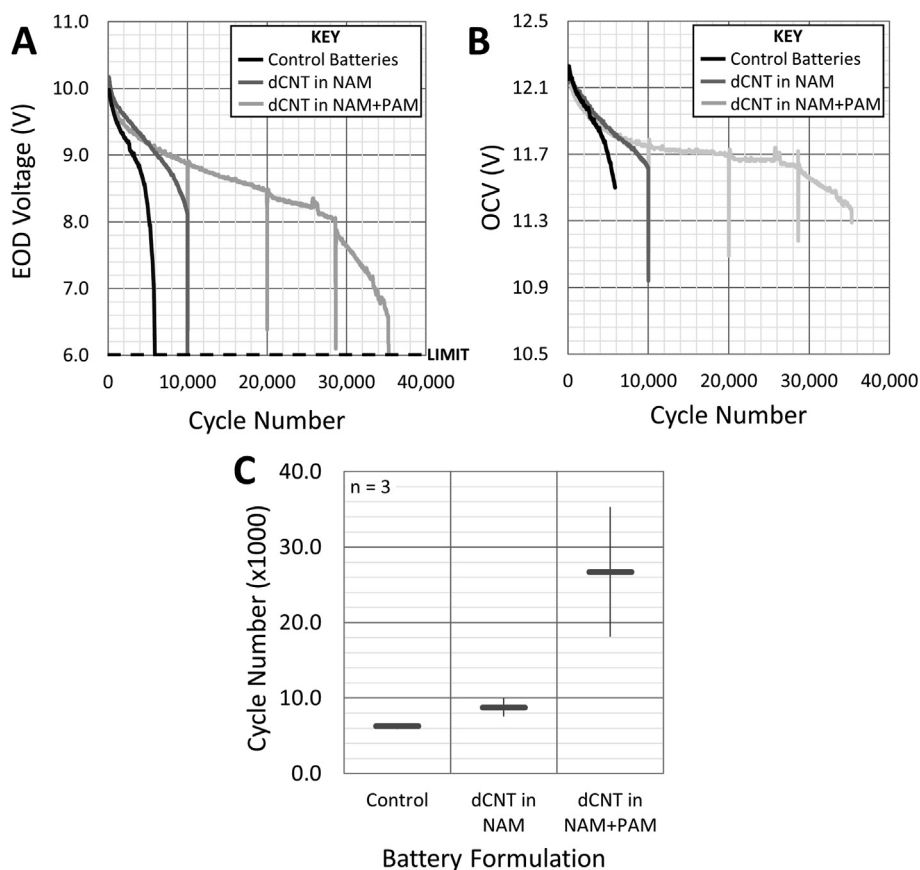


Fig. 9. Effect of dCNT on Cycle Life, SBA S0101. A, Discharge voltage curves retrieved from single batteries containing dCNT in various electrodes is shown with the 6.0 V limit indicated. Addition of dCNT to the negative electrode results in increased cycle life, but a larger effect is observed in batteries with dCNT in both electrodes. B, Charging voltages of each battery are shown. C, Data showing average cycle life of 3 batteries as horizontal bars with vertical bars drawn to encompass all data.

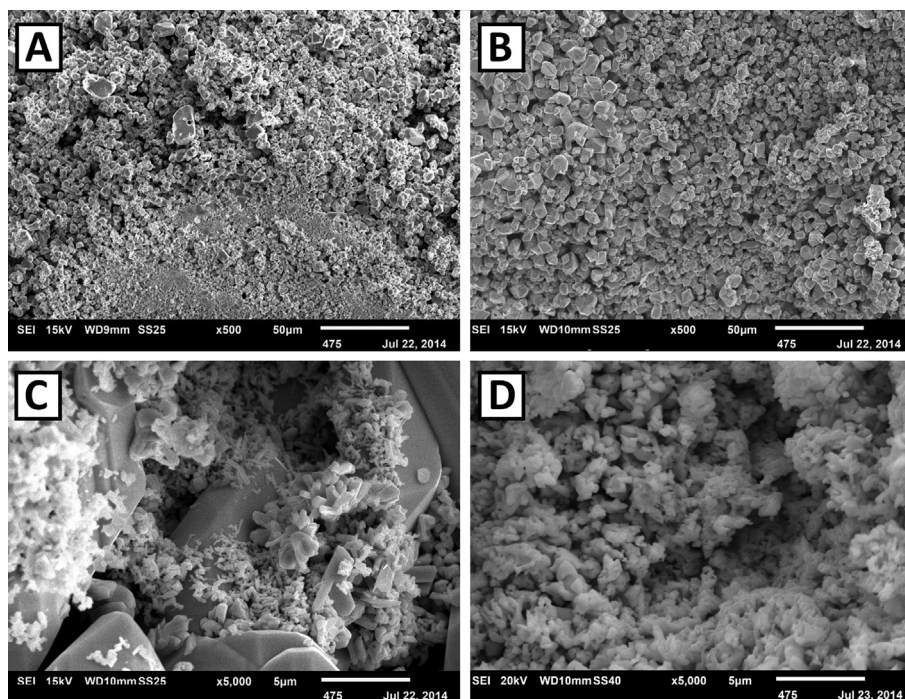


Fig. 10. SEM analysis of failed batteries from SBA Duty Cycles. A, Control, negative electrode showing a non-uniform structure and a variety of large and small crystals. B, dCNT containing, negative electrode showing highly uniform, small crystals. C, Control, positive electrode showing large, hard, well-defined crystals and a smattering of smaller crystals sitting atop. D, dCNT containing, positive electrode showing an active, slightly fluffly surface of homogenous composition.

relative size ($<2 \mu\text{m}$) and shape. Despite increased cycle numbers, micrographs of positive and negative electrodes containing dCNT appear to be in better condition than control electrodes. dCNT again appear to be influencing crystal size, shape, and integrity, but surface area and porosity measurements are required for validation of this theory.

Weight analyses show that control batteries lose 0.057 g/Cycle while batteries containing dCNT in the negative electrode lose 0.045 g/Cycle (20% decrease) and batteries containing dCNT in the negative and positive lose 0.025 g/Cycle (57% decrease).

dCNT incorporated into the negative, or negative and positive, electrodes dramatically increases the cycle life of batteries undergoing the SBA S0101 cycling test. Failure modes are altered and/or delayed while water loss is attenuated in the presence of dCNT.

4. Discussion

Several theories exist in the literature to explain the action of carbon in lead acid battery materials, but none can sufficiently explain *all* of our observations. Carbon is often claimed to act as a supercapacitive element within the lead electrode which can rapidly store a sudden influx of charging energy and then disperse it to the lead active material [17–20]. Alternatively, many advanced carbons have high surface areas, upwards of $1200 \text{ m}^2 \text{ g}^{-1}$, and some literature suggests that this high surface area can be conferred to the lead electrode to increase active material utilization [8]. It is unclear if this high surface area is a direct effect of carbon instigating higher surface area lead crystals, or simply the averaging of high surface area carbon combined with low surface area lead. Steric hindrance is also identified as a potential mechanism of carbon action where particles of carbon physically prevent the growth of large, inconvertible lead sulfate deposits to elongate cycle life [8]. A related theory involves carbon acting as a conductive pathway around nonconductive, inconvertible lead sulfate

deposits to ensure that a greater portion of the active material remains electronically accessible late into life [3]. Pavlov has designed a theory whereby carbon acts as a preferred surface for lead deposition and nucleation during cycling which acts to retain various lead components in small, easily convertible crystal forms to elongate cycle life [10,22]. A final theory of action portrays carbon as an undesirable additive: an oxygen-consuming component which instigates the loss of water through H_2 and CO_2 production [23].

Of these existing theories, surface-area enhancement comes the closest to explaining our observed dCNT results. As seen in Fig. 8, dCNT in the negative electrode produce significantly smaller crystal morphologies than control electrodes during HRPSoC cycling. Smaller, tighter crystal shapes are similarly seen during SBA cycling (Fig. 10). dCNT, it seems, are affecting lead crystal geometries during cycling. To prove this hypothesis, surface area and porosity measurements need to be made since extrapolation of these parameters from SEM micrographs is impossible. Among carbon additives, dCNT are unique because of the level of distribution they reach within the battery electrode. dCNT uniformity within the active material ensures that potential surface area or porosity augmentations are systemic, affecting the entire electrode instead of just the material in direct contact with the carbon. Although surface area augmentation explains some of our data, it does not explain *all* the data; changes to formation profiles, decreased water loss during cycling, polarization characteristics, and gas evolution properties are left unaddressed.

To answer this challenge, we introduce a new hypothesis which we are actively investigating: the dCNT/ H_{ad} Overcharge Reaction Mechanism. At its core, our hypothesis posits that the surface of dCNT could act as a transient storage medium for adsorbed hydrogen (H_{ad}). A quickly-mobilizable supply of high-powered reducing agents, such as these H_{ad} , could explain many of our observations regarding the performance of dCNT in the negative

electrode of lead acid batteries. In the positive electrode, where hydrogen production is thermodynamically disfavored, dCNT may be fulfilling a different function, potentially one involving mechanical or material strength improvements as opposed to electrochemical enhancements.

Atomic Hydrogen (H^+) can be adsorbed (H_{ad}) onto a variety of surfaces where it has the potential to evolve into molecular hydrogen (H_2). These reactions are described by a combination of the Volmer, Heyrovsky, and Tafel mechanisms. On the lead surface, a Volmer–Tafel mechanism is preferred. In this mechanism, the electron transfer resulting in H_{ad} is the slow, rate-determining step (Eq. 1 – Volmer Rxn) and the recombination of two H_{ad} atoms to produce H_2 is fast (Eq. 2 – Tafel Rxn):

$$H^+ + e^- + \text{Surface} \leftrightarrow \text{Surface} \cdot H_{ad} \text{ (Eq. 1 – Volmer Rxn, Fast on dCNT, Slow on Pb)}$$

$$2 \text{Surface} \cdot H_{ad} \leftrightarrow \text{Surface} + H_2 \text{ (Eq. 2 – Tafel Rxn, Preferred on Pb)}$$

On the dCNT surface, earlier studies indicate that hydrogen adsorption and evolution occur primarily by the Volmer–Heyrovsky mechanism [24]. In this mechanism, a fast, adsorptive, equilibrium step (Eq. 1 – Volmer Rxn) is followed by a slower, rate-determining electrochemical step (Eq. 3 – Heyrovsky Rxn) during which the adsorbed hydrogen (H_{ad}) reacts with an electron (e^-) and proton (H^+) to produce molecular hydrogen (H_2):

$$H^+ + e^- + \text{Surface} \leftrightarrow \text{Surface} \cdot H_{ad} \text{ (Eq. 1 – Volmer Rxn, Fast on dCNT, Slow on Pb)}$$

$$\text{Surface} \cdot H_{ad} + H^+ + e^- \leftrightarrow \text{Surface} + H_2 \text{ (Eq. 3 – Heyrovsky Rxn, Preferred on dCNT)}$$

During charging situations, therefore, a certain concentration of H_{ad} transiently exists in negative electrodes containing dCNT whereas none exists in control negative electrodes. Given the well-dispersed nature of dCNT throughout the active material, their hydrogen adsorptive/desorptive properties can be utilized uniformly across the electrode, even at the low concentrations presented here; a crucial tenet to our hypothesis.

The following discussion points portray all of our observations regarding dCNT-based lead acid battery performance improvements in the light of our new hypothesis:

1. Observation: dCNT Reduces Crystal Size during Curing [11]. The well-dispersed nature of dCNT within the electrode remains a fundamental concept to our hypothesis. During curing, it is possible that dCNT can act as a nucleation agent throughout the paste material. The uniformity of dCNT throughout the electrode could ensure that the majority of lead particles are close to a molecule of dCNT and, in some way, feeling its effects which may include H_{ad} trapping and release.
2. Observation: dCNT Extend the Time to Reach ToC during formation. During formation, immediately after conversion of the negative cured material, the battery reaches gas evolution voltage, also known as the Top of Charge Voltage (ToCV). At this voltage, control batteries evolve hydrogen slowly by the Volmer–Tafel mechanism while batteries containing dCNT evolve hydrogen quickly by the Volmer–Heyrovsky mechanism. The Volmer–Heyrovsky mechanism involves the underpotential deposition of hydrogen on the dCNT surface and, perhaps, their interior walls. This potential occurs more anodic to the potential at which hydrogen evolves on the lead surface, but more cathodic to the lead/lead sulfate reaction. Electrical energy will therefore be consumed, or stored as H_{ad} , on the dCNT until its

surface reaches a currently unknown saturation point. Such energy storage could explain the drop in ToCV exhibited when dCNT are included in the negative electrode and the delay in reaching the ToCV.

3. Observation: dCNT Alter the Constant-Voltage Polarization Test Characteristics. The initial, high-current spike during constant-voltage overcharging may be explained by the dCNT ability to rapidly store H_{ad} during charging. A faradaic process such as this could give the effect of pseudocapacitance in electrodes containing dCNT. Furthermore, the ability of batteries infused with dCNT to pass higher current at lower voltages and 100% SoC serves as a warning for constant-voltage charging situations and various gassing test protocols which typically employ such charging schemes. In these examples, dCNT batteries will absorb significantly more A·h than control batteries. The majority of this energy will feed gassing and water loss reactions which correlates with the gassing test results presented here.
4. Observation: dCNT Alter the Constant-Current Polarization Test Characteristics and Decrease the Tafel Slope. Reduction in the Tafel slope could be interpreted as evidence for a fast, low-overpotential process, such as the Volmer–Heyrovsky mechanism, taking precedence over a slower, high-overpotential process, such as the Volmer–Tafel mechanism, which would explain the decreased overvoltage requirements of the side reactions in dCNT batteries.
5. Observation: dCNT Increase Cycle Life in both HRPSoc and SBA. Both the cycle life tests reported here employ high current, high frequency pulses which, according to our hypothesis, could ensure that a portion of H_{ad} is constantly present on a layer of the dCNT within the electrode. The H_{ad} , if present, could provide more efficient usage of charging energy by rapidly accepting the energy and then donating it to the lead active material. Again, because of the uniform dispersion of dCNT throughout the electrode, this 2-step energy storage mechanism should be functioning plate wide. Since dCNT exist between lead sulfate crystals (and all other crystals), they may also assist in maintaining crystal structure throughout battery life and provide steric hindrance to lead sulfate crystal growth, even at open circuit.
6. Observation: dCNT Change the Crystal Structure/Topology of Cycled Plates. During cycling, crystal structure could be maintained by the H_{ad} which may be capable of directly converting lead sulfate to lead (Eq. 4) or keeping crystal sizes small through more efficient use of the charge/recharge energy.

$$2 \text{dCNT} \cdot H_{ad} + \text{PbSO}_4 \leftrightarrow \text{H}_2\text{SO}_4 + \text{Pb} + \text{dCNT} \text{ (Eq. 4 – dCNT}/H_{ad} \text{ Conversion Rxn)}$$

In these ways, transient hydrogen adsorption could explain *all* of our reported results. Although other CNT may be capable of performing some of these roles, only dCNT are capable of performing them uniformly, and completely, across the entire electrode so that the entire lead matrix feels their effect, even at low dCNT loading concentrations (0.16%). The quality of the dCNT dispersion through the matrix is fundamental to our interpretation of our dCNT/ H_{ad} Overcharge Reaction Mechanism. The dCNT/ H_{ad} hypothesis is far from proven, requiring significant research and fine tuning before more general acceptance. A full investigation of the hypothesis, supported with appropriate experimentation and analysis, will be the subject of our next report.

5. Conclusions

Presented here is an ongoing study of Molecular Rebar[®] Lead Negative and Positive, new negative and positive electrode additives comprised of discrete carbon nanotubes (dCNT).

Previously, dCNT were considered only as negative electrode additives but the work presented here proves their utility in the positive electrode. Owing to the material's formulation, it can be incorporated into battery pastes with no change to rheology or density, and, because of this, requires no changes to existing production lines. Batteries containing dCNT perform well in Reserve Capacity tests, produce performance gains in certain Cold-Cranking parameters, accept more current in cold conditions, and have favorable polarization profiles. dCNT increase the amount of gassing in standard tests designed for less efficient, poorly-charging batteries. Evidence presented here indicates that this increase in gassing is controllable with changes to either the test specifications (decreased voltage) or battery management systems (A·h control), akin to the alterations made during the transition from antimony to calcium grids. In two life-cycle models, the inclusion of dCNT into battery electrodes increases cycle life by 60% (HRPSOC) or up to 500% (SBA). Teardown analyses of batteries which reached life cycle test limits indicate that failure mechanisms reside in the negative electrode for batteries undergoing HRPSOC duty cycles and in the separator for batteries undergoing SBA duty cycles. Theories of dCNT mechanism of action are discussed and a new, possibly controversial hypothesis is introduced: dCNT/H_{ad} Overcharge Reaction Mechanism. The new hypothesis will form the basis of our next report and is presented here as a point for discussion, only.

Future research investigating the effects of dCNT in batteries will include comparison of the data in flooded batteries and VRLA batteries, comparison of batteries utilizing antimony alloy grids to batteries utilizing calcium alloy grids, additional life cycle tests, and optimization of dCNT formulations and loading percentages.

Acknowledgments

The authors sincerely thank Kurt W. Swogger and Dr. Clive P. Bosnyak for their patronage as well as the many helpful discussions which made this research possible. The authors would also like to thank Michael Gauthier, Doug Hunter, and Russell Turner for their assistance in preparing the Molecular Rebar[®] Lead Negative and Positive used in this study and Dr. Jeremy Meyers for his aid in

preparing the final report. Finally, the authors thank Mr. Vinal V. Deo and Mr. Tula Ram who provided assistance for testing the batteries at Pacific Batteries, Ltd.

Appendix A. Supplementary data

Supplementary data related to this article can be found at <http://dx.doi.org/10.1016/j.jpowsour.2014.12.117>.

References

- [1] J. Dambrowski, in: Deutronic Elektronik GmbH, Adlkofen, 2009, pp. 1–16. Available at: http://www.deutronic.com/fileadmin/images/PDF/Ladegeraete/deutronic-lader_eng.pdf (accessed 03.11.14.).
- [2] K. Nakamura, M. Shiomi, K. Takahashi, M. Tsubota, J. Power Sources 59 (1996) 153–157.
- [3] M. Shiomi, T. Funato, K. Nakamura, K. Takahashi, M. Tsubota, J. Power Sources 64 (1997) 147–152.
- [4] W.J. Murray, S.F. Malo, in: 2011 NDIA Ground Vehicle Systems Engineering and Technology Symposium, Dearborn, Michigan, 2011.
- [5] J. Valenciano, A. Sanchez, F. Trinidad, A.F. Hollenkamp, J. Power Sources 158 (2006) 851–863.
- [6] D.P. Boden, D.V. Loosmore, M.A. Spence, T.D. Wojcinski, J. Power Sources 195 (2010) 4470–4493.
- [7] D.G. Enos, S.R. Ferreira, R. Shane, in: Scandia National Laboratories, Albuquerque, (2011). Available at: <http://prod.sandia.gov/techlib/access-control.cgi/2011/118263.pdf> (accessed 03.11.14.).
- [8] K. Micka, M. Calabek, P. Baca, P. Krivak, R. Labus, R. Bilko, J. Power Sources 191 (2009) 154–158.
- [9] M. Saravanan, P. Sennu, M. Ganesan, S. Ambalavanan, J. Electrochem. Soc. 160 (2013) A70–A76.
- [10] D. Pavlov, T. Rogachev, P. Nikolov, G. Petkova, J. Power Sources 191 (2009) 58–75.
- [11] S.W. Swogger, P. Everill, D.P. Dubey, N. Sugumaran, J. Power Sources 261 (2014) 55–63.
- [12] K.W. Swogger, C.P. Bosnyak, in: 70th Annual Technical Conference of the Society of Plastics Engineers, Curran Associates, Inc, Orlando, Florida, 2012, pp. 448–451.
- [13] R. Shapira, G.D. Nessim, T. Zimrin, D. Aurbach, Energy Environ. Sci. 6 (2013) 587–594.
- [14] D.P. Boden, J. Power Sources 73 (1998) 89–92.
- [15] D. Pavlov, P. Nikolov, J. Electrochem. Soc. 159 (2012) A1215–A1225.
- [16] K. Nakano, S. Takeshima, J. Furukawa, in: Furukawa Review, 2007, pp. 49–55.
- [17] J. Xiang, P. Ding, H. Zhang, X. Wu, J. Chen, Y. Yang, J. Power Sources 241 (2013) 150–158.
- [18] D. Pavlov, P. Nikolov, J. Power Sources 242 (2013) 380–399.
- [19] M. Fernandez, J. Valenciano, F. Trinidad, N. Munoz, J. Power Sources 195 (2010) 4458–4469.
- [20] P.T. Moseley, J. Power Sources 191 (2009) 134–138.
- [22] D. Pavlov, P. Nikolov, T. Rogachev, J. Power Sources 195 (2010) 4444–4457.
- [23] K.R. Bullock, J. Power Sources 195 (2010) 4513–4519.
- [24] P.P. Prosini, A. Pozio, S. Botti, R. Ciardi, J. Power Sources 118 (2003) 265–269.